Structural Dynamics
co-published by AIP Publishing | ACA

NOW INDEXED IN THOMSON REUTERS DATABASES

Communication: X-ray coherent diffractive imaging by immersion in nanodroplets

Rico Mayro P. Tanyag, Charles Bernando, Curtis F. Jones, Camila Bacellar, Ken R. Ferguson, Denis Anielski, Rebecca Boll, Sebastian Carron, James P. Cryan, Lars Englert, Sascha W. Epp, Benjamin Erk, Lutz Foucar, Luis F. Gomez, Robert Hartmann, Daniel M. Neumark, Daniel Rolles, Benedikt Rudek, Artem Rudenko, Katrin R. Siefermann, Joachim Ullrich, Fabian Weise, Christoph Bostedt, Oliver Gessner, and Andrey F. Vilesov

Articles you may be interested in

Development of an adaptable coherent x-ray diffraction microscope with the emphasis on imaging hydrated specimens
Rev. Sci. Instrum. **84**, 113702 (2013); 10.1063/1.4828656

Influence of Noise and Missing Data on Reconstruction Quality in Coherent X-ray Diffractive Imaging
AIP Conf. Proc. **1365**, 305 (2011); 10.1063/1.3625365

Bragg Coherent Diffraction Imaging of Epitaxial Nanostructures Using Focused Hard X-ray Ptychography
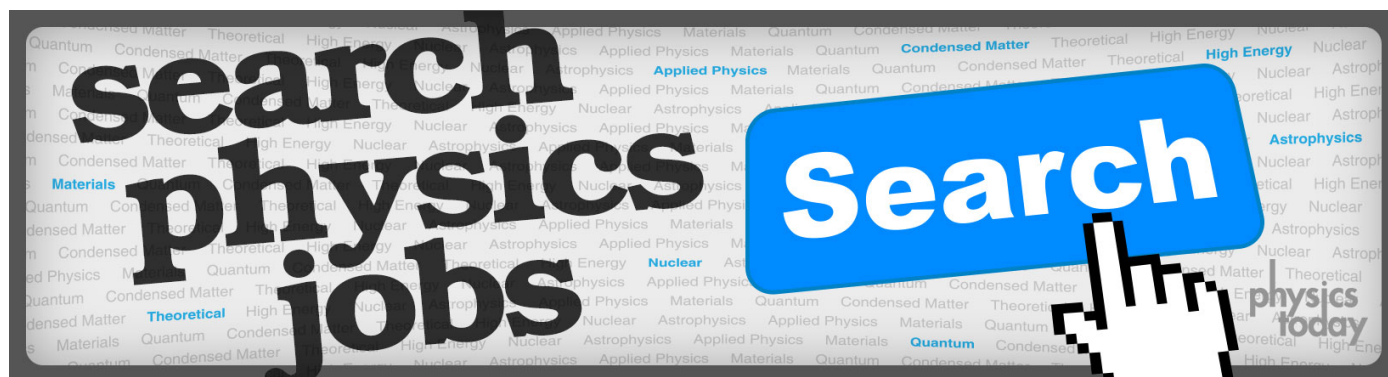AIP Conf. Proc. **1365**, 235 (2011); 10.1063/1.3625347

Coherent Diffractive Imaging with X-rays and Electrons
AIP Conf. Proc. **705**, 1372 (2004); 10.1063/1.1758057

Coherent high energy X-ray optics for imaging, diffraction and spectroscopy
AIP Conf. Proc. **507**, 76 (2000); 10.1063/1.1291122

Communication: X-ray coherent diffractive imaging by immersion in nanodroplets

Rico Mayro P. Tanyag,[1] Charles Bernando,[2] Curtis F. Jones,[1]
Camila Bacellar,[3,4] Ken R. Ferguson,[5] Denis Anielski,[6,7] Rebecca Boll,[6,7,8]
Sebastian Carron,[5] James P. Cryan,[3] Lars Englert,[9] Sascha W. Epp,[6,7,a)]
Benjamin Erk,[6,7,8] Lutz Foucar,[7,10] Luis F. Gomez,[1,b)] Robert Hartmann,[11]
Daniel M. Neumark,[3,4] Daniel Rolles,[7,8,10,12] Benedikt Rudek,[6,7,c)]
Artem Rudenko,[6,7,12] Katrin R. Siefermann,[3,d)] Joachim Ullrich,[6,7,c)]
Fabian Weise,[3,e)] Christoph Bostedt,[5,13,14,f)] Oliver Gessner,[3,f)] and
Andrey F. Vilesov[1,2,f)]

[1]*Department of Chemistry, University of Southern California, Los Angeles,
California 90089, USA*
[2]*Department of Physics and Astronomy, University of Southern California, Los Angeles,
California 90089, USA*
[3]*Chemical Sciences Division, Lawrence Berkeley National Laboratory, Berkeley,
California 94720, USA*
[4]*Department of Chemistry, University of California Berkeley, Berkeley, California 94720, USA*
[5]*Linac Coherent Light Source, LCLS, SLAC National Accelerator Laboratory,
2575 Sand Hill Road, Menlo Park, California 94025, USA*
[6]*Max-Planck-Institut für Kernphysik, Saupfercheckweg 1, 69117 Heidelberg, Germany*
[7]*Max Planck Advanced Study Group at the Center for Free-Electron Laser Science (CFEL),
Notkestraße 85, 22607 Hamburg, Germany*
[8]*Deutsches Elektronen-Synchrotron (DESY), Notkestraße 85, 22607 Hamburg, Germany*
[9]*Max-Planck-Institut für extraterrestrische Physik, Giessenbachstraße, 85741 Garching,
Germany*
[10]*Max-Planck-Institut für Medizinische Forschung, Jahnstrasse 29, 69120 Heidelberg,
Germany*
[11]*PNSensor GmbH, Otto-Hahn-Ring 6, 81739 München, Germany*
[12]*J.R. MacDonald Laboratory, Department of Physics, Kansas State University, Manhattan,
Kansas 66506, USA*
[13]*Argonne National Laboratory, 9700 South Cass Avenue B109, Lemont, Illinois 60439, USA*
[14]*Department of Physics and Astronomy, Northwestern University, 2145 Sheridan Road,
Evanston, Illinois 60208, USA*

Lensless x-ray microscopy requires the recovery of the phase of the radiation scattered from a specimen. Here, we demonstrate a *de novo* phase retrieval technique by encapsulating an object in a superfluid helium nanodroplet, which provides both a physical support and an approximate scattering phase for the iterative image reconstruction. The technique is robust, fast-converging, and yields the complex density of the immersed object. Images of xenon clusters embedded in superfluid helium droplets reveal transient configurations of quantum vortices in this fragile system. © *2015 Author(s). All article content, except where otherwise noted, is licensed under a Creative Commons Attribution 3.0 Unported License.*
[http://dx.doi.org/10.1063/1.4933297]

a)Present address: Max-Planck-Institut für Struktur und Dynamik der Materie, Luruper Chausee 149, D-22761 Hamburg, Germany.
b)Present address: New Focus, 3635 Peterson Way, Santa Clara, California 95054, USA.
c)Present address: Physikalisch-Technische Bundesanstalt, Bundesallee 100, D-38116 Braunschweig, Germany.
d)Present address: Leibniz Institute of Surface Modification (IOM), Permoserstraße 15, 04318 Leipzig, Germany.
e)Present address: Berliner Glas KGaA Herbert Kubatz GmbH and Co., Waldkraiburger Str. 5, 12347 Berlin, Germany.
f)Authors to whom correspondence should be addressed. Electronic addresses: cbostedt@anl.gov; ogessner@lbl.gov; and vilesov@usc.edu.

X-ray coherent diffractive imaging (CDI) is a lensless microscopy technique for obtaining the density distribution of a non-periodic object from its diffraction image.[1–4] The advent of x-ray free electron lasers (XFEL) has enabled the recording of high quality diffraction images using single, intense, sub-100 fs pulses. CDI provides previously unattainable imaging information of single nanoparticles and biological specimens,[5,6] and of transient intermediates such as flash-excited building blocks of photosynthetic systems.[7] In particular, single-shot CDI may revolutionize the investigation of nanostructures and of rare transient events that are otherwise lost in the statistical sampling of time-averaged measurements.

Diffraction images represent the moduli squared of the complex scattering amplitudes. CDI techniques are based on the conjecture that the scattering phases can be retrieved from oversampling the recorded diffraction patterns.[1,2] However, a unique phase retrieval remains challenging in practice due to ambiguities induced by unknown overall object extensions ("support"), signal noise, and missing data due to detector limitations. As a result, iterative transform algorithms (ITA)[8,9] such as error-reduction (ER) and hybrid input-output (HIO) have been established to bridge between the experimental data and the mathematical paradigm of oversampling theorem. The missing scattering phase information is usually reconstructed based on self-consistency arguments, such as a good agreement between the Fourier transformation of the obtained densities and the measured diffraction amplitudes, along with the application of various physical constraints to minimize the sampled phase space and to prevent trapping of the algorithms in local minima. Trapping and the associated problem of non-unique reconstructions pose a recurring challenge for ITAs. For example, a commonly used shrink-wrap technique is capable of finding the support of an object against a zero background.[10] However, the calculated object density is represented by an average of hundreds of independent reconstruction runs, each with thousands of iterations.[11–13] Such a procedure is computationally expensive and usually incompatible with real-time data analysis.[14] The common practice of performing large numbers of reconstruction runs, where "acceptable" runs are averaged and "failed" runs are discarded, may also contribute to reconstruction ambiguity and loss of resolution.

Here, we present a new approach to single-shot CDI that is based on immersing specimens in nanodroplets, henceforth referred to as droplet coherent diffractive imaging (DCDI). The droplets serve as vehicles to deliver and localize the targets in the x-ray focus, define the sample support, and act as x-ray reference scatterers that provide an approximate solution to the phase problem. We demonstrate that DCDI is an efficient and robust reconstruction technique that converges to physically meaningful solutions within minutes of single central processing unit (CPU) computing times. This work was motivated by our study of quantum vortices in sub-micron sized superfluid He droplets. Foreign atoms and clusters are attracted to the vortex cores and form extended nanoscale structures, which can be visualized by using various imaging techniques.[15–20] In our most recent study, single micron-sized doped droplets revealed characteristic Bragg patterns in x-ray diffraction, which were assigned to lattices containing up to ≈ 200 quantum vortices.[20] Here, we focus on the retrieval of the "snapshots" of shapes and positions of few vortices from diffraction patterns devoid of any Bragg spots.

The experimental layout is depicted in Fig. 1. Droplets were formed along the free jet expansion of helium from a 5 μm nozzle cooled to about 5 K.[20–22] The droplets considered in this work have a radius of $\sim$300 nm and consist of approximately 10^9 He atoms ($N_{He} = 94 \times R(\text{nm})^3$). Each droplet was doped with many ($\approx 10^6$) Xe atoms that condensed into groups of clusters. The doped droplets were illuminated by a focused (≈ 25 μm^2) x-ray beam ($h\upsilon = 1.5$ keV, $\lambda = 0.826$ nm, $\approx 10^{12}$ photons per 100 fs pulse, repetition rate 120 Hz), and the scattered x-rays were detected at small scattering angles (<0.05 rad) on a shot-by-shot basis using a cooled pnCCD detector containing 1024×1024 pixels of 75×75 μm^2 in size.[23–25] The distance from the scattering center to the detector was 0.565 m.

Representative single-shot diffraction images of Xe-doped He nanodroplets are displayed in Figs. 2(a1)–2(c1) in a logarithmic color scale. Each image exhibits a periodic radial intensity modulation that represents the characteristic concentric ring structure of the diffraction patterns from the nearly spherical host droplets. Diverse speckle patterns are superimposed on these rings due to the interference between waves scattering off the He droplets and the embedded
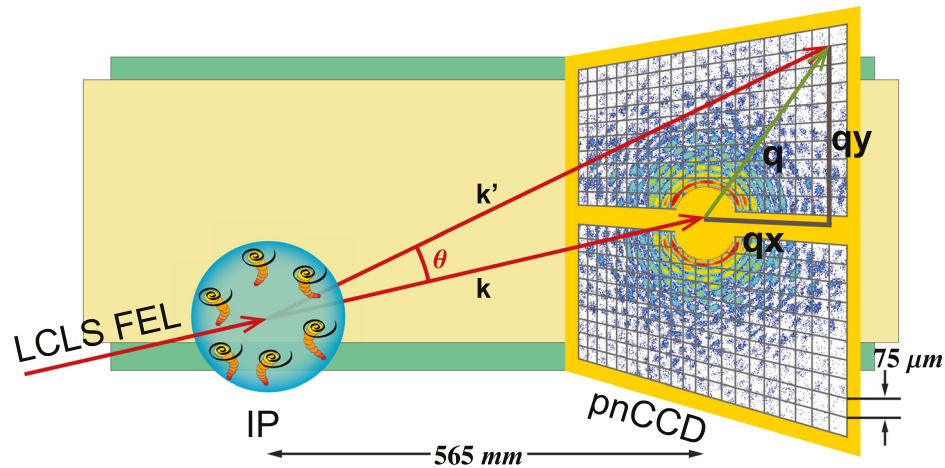
FIG. 1. Experimental setup. Diffraction images of extended nanoscale objects are recorded upon immersion in superfluid helium nanodroplets that are irradiated with single XFEL pulses. The optically thin droplet serves both as the object support and a reference scatterer.

Xe structures. Using the DCDI algorithm, which will be explained in detail below, density profiles of the Xe clusters inside the droplet are obtained and displayed in Figs. 2(a2)–2(c2) in a linear color scale. The black circles mark the droplet contours that correspond to the boundaries
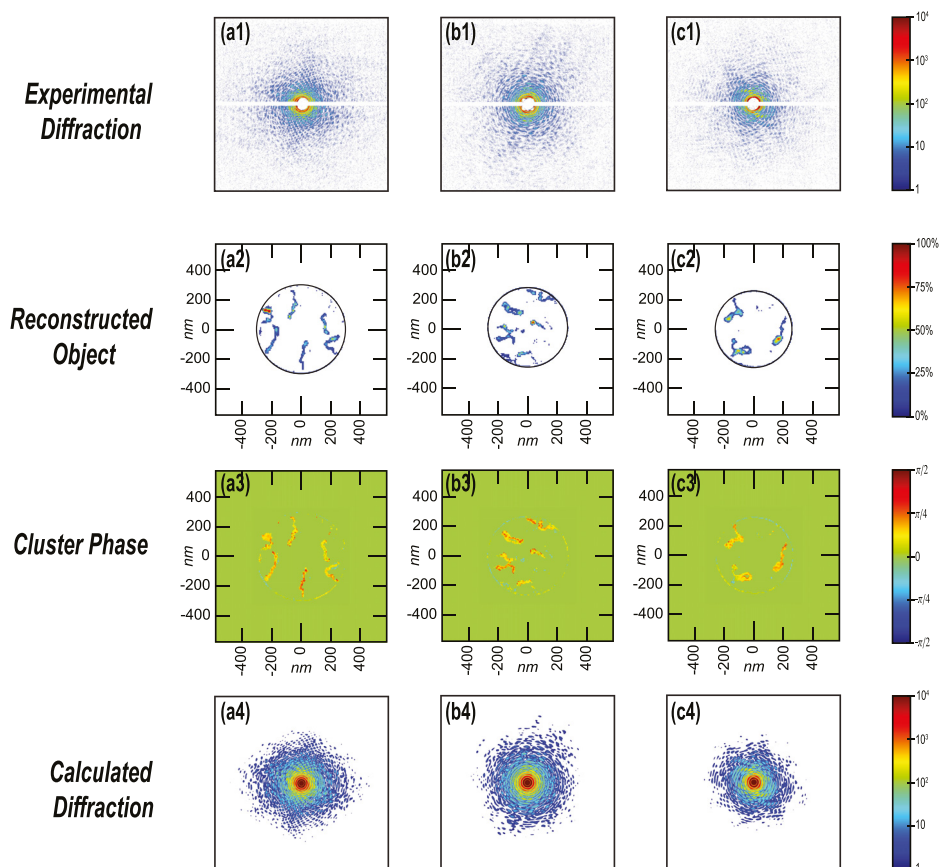

FIG. 2. Diffraction images and DCDI reconstructions. (a1)–(c1) Experimental diffraction images of Xe-doped droplets (radius ∼ 300 nm). (a2)–(c2) DCDI reconstructions of Xe clusters assembled inside the droplets and droplet contours. (a3)–(c3) Phases of the complex cluster densities. (a4)–(c4) Calculated diffraction images corresponding to the reconstructed total densities (Xe clusters and He droplets).

of the support. The phase profiles of the reconstructed complex densities are shown in Figs. 2(a3)–2(c3) in a linear color scale ranging from $-\pi/2$ to $\pi/2$. Figures 2(a4)–2(c4) display calculated diffraction images derived from the reconstructed total densities, i.e., droplet densities plus Xe densities, in a logarithmic color scale. The calculated diffraction images closely resemble the measured data and smoothly fill areas where experimental intensities are missing. Differences at large distances from the detector center can be accounted for by the discrete nature of photons in the measured diffraction patterns, whereas light waves in the calculations are continuous. Additional parameters such as the droplet dimensions, total He densities, and total Xe densities are included in Table S1 of the supplementary material.[26] We have selected images containing only circular diffraction patterns for this work, i.e., with aspect ratios within 2% of unity. Such patterns correspond to either spherical droplets or spheroidal droplets imaged along the principal axis. A considerable fraction (40%) of the droplets in the beam have elliptical diffraction patterns and stem from rotating droplets experiencing noticeable centrifugal deformation.[20] The DCDI algorithm is also applicable to spheroidal droplets, but this is beyond the scope of this work. In addition, the surface of the droplets may also be impacted by shape oscillations but these typically decay within 4 ms of flight time,[20] long before the droplets reach the XFEL interaction region.

The DCDI algorithm is based on the ER algorithm[8] that has been modified to include a preset He droplet density and size. A flow diagram of the algorithm is illustrated in Fig. 3. In small-angle scattering, diffraction images can be approximately calculated from the two-dimensional density projection of an object onto the detector plane (X-Y). For a spherical helium droplet with radius, R, the projection of the density, ρ_{He}, is given by

$$\rho_{x,y}^{He} = C \times \sqrt{1 - \frac{x^2 + y^2}{R^2}}. \tag{1}$$

The determination of R and the density scaling factor, C, are detailed in the supplementary material.[26] The algorithm is initiated using a predefined droplet density, ρ_{input}, as expressed by Eq. (1). After Fourier transform, the modulus of the scattering amplitude is replaced by the square root of the measured intensity, I_{Meas}, whereas the phase, φ, is retained. This intermediate scattering amplitude is called G'. For reciprocal space regions that lack experimental intensity
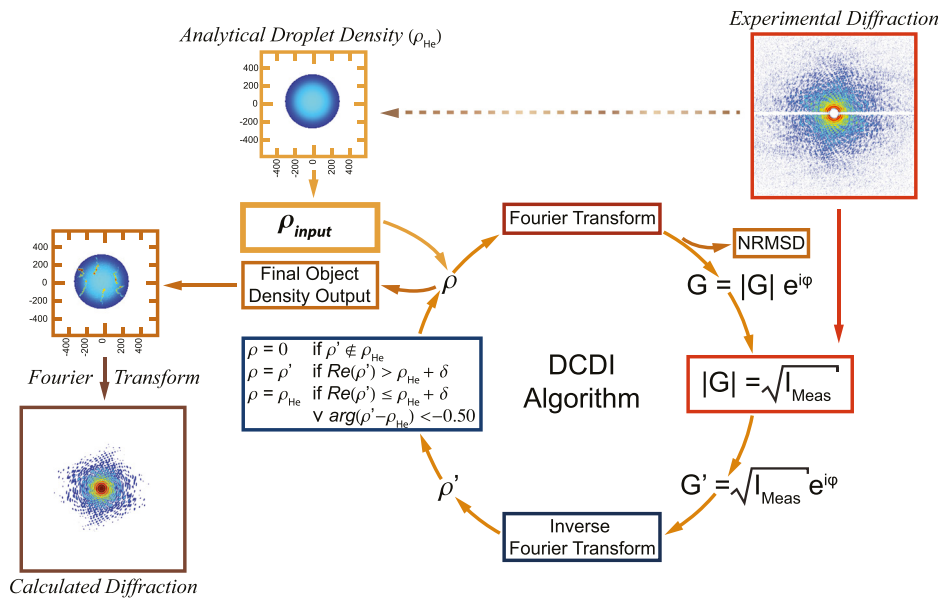

FIG. 3. Schematic of droplet coherent diffractive imaging (DCDI). The algorithm is initiated using a preset He droplet density ρ_{input}. Series of (inverse) Fourier transforms between object- and reciprocal-space with iterative reinforcement of constraints in both spaces rapidly converge to yield the density of Xe clusters inside the droplet.

information (such as the region of the central detector hole, the gap between the detector plates, and some arrays of damaged pixels), the algorithm retains the complex scattering amplitude obtained from the Fourier transform of the object density, ρ. An approximate solution, ρ', for the combined density of the He droplet and the embedded dopants is estimated from the inverse Fourier transform of G'. This density ρ' is adjusted to a new trial solution of ρ by applying several constraints. ρ' is set to zero for points outside the droplet boundary (black circles in Figs. 2(a2)–2(c2)). If the real part of ρ' inside the droplet contour exceeds ρ_{He} by a predetermined threshold value, δ, the algorithm retains ρ'; otherwise, ρ' is replaced with ρ_{He}. This step discerns between image contributions from the host droplet and the immersed objects. The calculations in Fig. 2 were performed with $\delta = 5000$, see supplementary material[26] for unit conventions and the derivation of δ. If the argument of the complex quantity $\rho' - \rho_{He}$ is less than -0.50 rad, ρ' is also replaced with ρ_{He}. This mild phase constraint effectively amplifies one of the complex conjugate solutions (i.e., one with positive imaginary part), which accelerates convergence and suppresses trapping of the algorithm in center-symmetric configurations, see examples in the supplementary material.[26]

Figure 4 illustrates the rapid convergence of DCDI for the data displayed in Fig. 2(a1). The algorithm usually identifies the main object features within a few iterations and completely converges within less than 100 iteration cycles. As shown in Fig. 4(g), the normalized root mean square deviation (NRMSD)[26] of the diffraction intensity converges within less than 20 iterations. The NRMSD value remains constant within 0.1% after 100 iterations for which the DCDI algorithm requires about 5 min of CPU time on a standard personal computer. In contrast, application of traditional ER or HIO algorithms[8,9] with the droplet's outline as a support did not resolve the filaments. Instead, the algorithms converged to a solution having a large non-physical amplitude variation of the helium droplet density. Furthermore, reconstructions from these algorithms often exhibit sharp discontinuities in regions where experimental intensities were unavailable. DCDI was coded using the Mathcad® software package. Both object and reciprocal spaces were sampled with 981×981 matrices. Based on the scattering geometry and wavelength, the size of a single pixel is 6.35 nm and 1.01×10^{-3} nm^{-1} (about 0.133 mrad) in the object and Fourier domains, respectively.

The density distributions in Figs. 2(a2)–2(c2) show that the embedded Xe atoms neither form a single cluster nor are they dispersed randomly inside the droplet. Instead, they form filaments separated by about 100–200 nm. The formation of the filaments is consistent with the condensation of dopant atoms onto the cores of quantum vortices as previously demonstrated in He droplets of 300 nm to 2000 nm in diameter.[15–20] Vortices with the same sense of rotation repel each other[27] and should give rise to widely spaced filaments symmetrically distributed around the droplet's center. For example, the image in Fig. 2(a2) is consistent with an approximately hexagonal pattern of C-shaped filaments imaged at some angle with respect to the symmetry axis. Similar symmetric arrangements of few parallel vortices in a rotating bucket filled
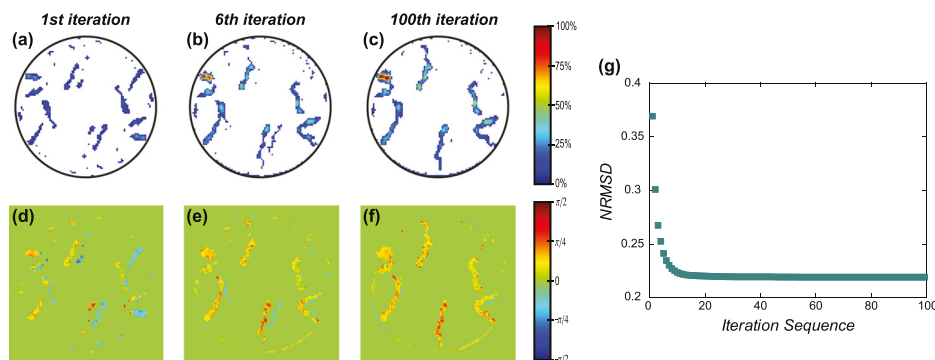

FIG. 4. Convergence of the DCDI algorithm. Most of the objects' density ((a)–(c)) and scattering phase ((d)–(f)) distributions are well approximated after a few iterations. Panel (g) shows the normalized root mean square deviation (NRMSD) between the measured and calculated diffraction signals at different numbers of iterations.

with superfluid helium have previously been observed by Packard and co-workers.[28] In comparison, the vortices in the droplets are expected to be curved as they must terminate perpendicular to the surface,[29,30] which is consistent with the observed curved filaments in Fig. 2. Similar wire-like structures were observed when doping the droplets with metal and metalloid atoms.[16–19] The clusters, in those experiments, were deposited on carbon films and were imaged via transmission electron microscopy. Therefore, we identify each of the observed clusters with the position of a vortex core. The good agreement of the obtained vortex configurations with previous experimental findings and theoretical predictions also substantiates the reliability of the DCDI reconstructions. Doping the droplet with Xe atoms facilitates the visualization of the vortex cores, which are otherwise challenging to detect. Each core has a diameter of only ∼0.2 nm,[31] which is about four orders of magnitude smaller than the typical He droplet dimension. The DCDI reconstructions also demonstrate the utility of ultrafast single-shot x-ray CDI to study irreproducible, transient systems. The ascertained vortex filament structures are not stationary but rotate in the lab frame at ∼10^7 rad/s;[20] thus, slower time-averaged measurements would blur the filament structures. In addition, the size, angular velocity, and axis of rotation of the droplets cannot be controlled, which would lead to a significant loss of information in ensemble–averaged experiments.

The known scattering amplitude of the host droplet facilitates the fast retrieval of the density of an unknown immersed object in DCDI. It is instructive to compare DCDI with Fourier Transform Holography (FTH), in which the hologram results from the interference between light waves emerging from the object and a small, spatially separated reference hole (ideally a point source[32,33]). In FTH, the Fourier transform of the diffraction intensity produces the autocorrelation functions of the object and the reference, as well as two complex conjugate cross-correlations of the object and the reference, which are the object images. In order to avoid any overlap of the reconstruction and the autocorrelation images, the reference hole must be placed more than three object radii away from the sample. It has been demonstrated, however, that reconstructions can still be accomplished with shorter object-reference distances by using ITAs.[34] Another variant of FTH surrounds the object of interest with specially designed reference structures.[35] While continued progress in extending FTH capabilities is being made,[36,37] its application in XFEL experiments remains challenging, mostly because the reference structure is destroyed with every single XFEL shot. The main difference between DCDI and FTH is that there is no separation between the object and the reference in DCDI; in fact, the droplet itself serves as both the reference and the object support. Each object in DCDI is contained within a reference droplet, since the droplets are the vessels that transport the objects to the scattering volume.

A He droplet is a particularly useful reference because it is optically thin with a refractive index of $n_{He} = (1 - 1.34 \times 10^{-5} + 1.6 \times 10^{-8}i)$ at 1.5 keV, yet it still produces sufficient x-ray scattering for the reconstruction;[20] the imaginary part of its scattering amplitude is negligible; it is a quantum liquid that weakly interacts with any immersed specimen; and it exemplifies the most homogeneous density possible.[31] It also has a naturally occurring spherical or spheroidal shape with a sub-nm sharp edge.[21] The droplet dominates the scattering amplitude, providing approximate phasing of the interferogram, which is the basis for the fast convergence of DCDI. In contrast, conventional CDI algorithms use random phases as a starting point. Since the droplet encloses the object in DCDI, the reconstructed density and its complex conjugate overlap, warranting application of ITAs, such as ER. ITA is also required to compensate for the missing diffraction data due to detector constraints. The smallest reconstructed feature is three pixels (18 nm) across, which is comparable to the theoretical CDI resolution of about $\lambda/\theta_{max} \approx 12$ nm, wherein θ_{max} is determined by the spatial extent of the detector.

Provided that the elemental (molecular) identity of the dopant is known, it is possible to obtain its absolute number of particles from a single image by using DCDI because the droplet and the contained object are exposed to the same x-ray flux. As an example, the density profile depicted in Fig. 2(a2) is used to obtain the total density of Xe as $1.87 \times 10^7 + 7.70 \times 10^6 i$, whereas the total He density from Eq. (1) is 1.38×10^9. The total density is proportional to $(f_1^0 + f_2^0 i) \cdot N_a$, in which f_1^0 and f_2^0 are the real and complex atomic scattering factors, and N_a is

the total number of scattering atoms. At 1.5 keV, the scattering factors are $f_1^0 = 2.0$, $f_2^0 = 2.4 \times 10^{-3}$ for He and $f_1^0 = 46.4$, $f_2^0 = 19.3$ for Xe.[38] Using the ratio of the real part of the densities of Xe, ρ_{Xe}, and He, ρ_{He}, and their corresponding f_1^0 factors, the total number of Xe is

$$N_{Xe,DCDI} = \frac{f_{1,He}^0 \times N_{He} \times \text{Re}(\rho_{Xe})}{f_{1,Xe}^0 \times \rho_{He}}. \tag{2}$$

For the configuration presented in Fig. 2(c2), the number of Xe atoms is $N_{Xe,DCDI} = 1.5 \times 10^6$, which agrees well with $(2.0 \pm 0.4) \times 10^6$ atoms derived from pickup kinetics, see Table S1 in the supplementary material.[26] This good agreement indicates that all Xe atoms can be accounted for in the DCDI reconstruction, which is facilitated by the high local density of the embedded structures that exceeds the value of δ. In general, the size of an imaged object (such as a cluster filament) should be substantially smaller than the host droplets. A poorer DCDI performance may be expected if the size of the object is comparable to the size of the droplet, such as in a homogeneous distribution of dopant atoms in the droplet. The absolute precision of determining the number of encapsulated Xe atoms in DCDI is directly related to the uncertainty in the value of C (Eq. (1)), which is about 10% for intense diffraction images ($\geq 5.0 \times 10^5$ scattered photons). The calculated number of atoms is also sensitive to the value of δ, see supplementary material.[26] In contrast, conventional CDI requires the determination of the absolute x-ray flux at the scattering point for absolute density measurements, which is usually impossible for single images due to the uncertainty of the object's position with respect to the tight focus of the XFEL beam.

DCDI also yields the absolute scattering phase of the studied atoms and, therefore, provides some degree of elemental specificity. For an optically thin object, each of its volume elements can be considered as an independent scattering center for the incident wave,[39] which constitutes the so-called Rayleigh-Gans approximation and holds if $\frac{S \cdot |n-1|}{\lambda} \ll 1$ (λ: wavelength of light; S: typical extension of the scattering object along the beam). The Rayleigh-Gans approximation is well satisfied for a He droplet with 300 nm radius, for which $\frac{2R \cdot |n_{He}-1|}{\lambda} \approx 0.01$. The refractive index of solid Xe at $h\nu = 1.5$ keV can be obtained[40] from the corresponding number density and atomic scattering factors to be $n_{Xe} = (1 - 2.46 \times 10^{-4} + 1.02 \times 10^{-4}i)$. The upper boundary of $\frac{S \cdot |n_{Xe}-1|}{\lambda}$ can be estimated from the maximum number of Xe atoms per pixel in Fig. 2(a2) ($\approx 10^4$) to be about 5×10^{-3}. Therefore, the effect of refraction from Xe is negligible, and the phase of the cluster density should be given by $\tan^{-1}(f_2^0/f_1^0)$ for Xe. As an example, the average complex phase of the Xe density in Fig. 2(a2) is $\varphi = 0.39$ rad, which is in excellent agreement with the value of $\varphi = 0.394$ rad deduced from the corresponding x-ray atomic scattering factors. Furthermore, if the phase is known *a priori*, as in the present case, it can be used as an additional constraint in object space to accelerate convergence, and to minimize the appearance of the complex conjugate image in the reconstruction. This is particularly useful for weak scattering signals.

We have demonstrated the application of DCDI algorithm for reconstructing the shapes of quantum vortices in a superfluid helium nanodroplet. Compared to other CDI techniques, the most prominent advantages of DCDI are: (i) a rapid convergence and shot noise resilience that may enable real-time image analysis during experiments; (ii) the determination of the absolute scattering phase, and (iii) the capability to derive absolute object densities from single-shot measurements. In the future, it will be interesting to expand DCDI reconstructions to a wider range of objects and dynamic phenomena. Helium droplets have been shown to readily pick up targets as large as ~12 000 Dalton sized proteins[41] and to support chemical transformations.[21] Combining these characteristics with DCDI may enable a new class of ultrafast single-shot imaging experiments that identify the structures of individual macromolecules or transient intermediates in chemical reactions. We also note that the algorithm could be extended to include external objects. In order to explore its generality, the DCDI technique should be applied to droplets of other materials (e.g., water) as well as to droplets on a surface (such as on a silicon

nitride window). The performance of the DCDI technique should also be independently validated by imaging test objects with known density distributions.

[1] J. Miao, D. Sayre, and H. N. Chapman, J. Opt. Soc. Am. A **15**, 1662 (1998).
[2] H. N. Chapman, A. Barty, S. Marchesini, A. Noy, S. R. Hau-Riege, C. Cui, M. R. Howells, R. Rosen, H. He, J. C. H. Spence, U. Weierstall, T. Beetz, C. Jacobsen, and D. Shapiro, J. Opt. Soc. Am. A **23**, 1179 (2006).
[3] H. N. Chapman and K. A. Nugent, Nat. Photonics **4**, 833 (2010).
[4] J. W. Miao, T. Ishikawa, I. K. Robinson, and M. M. Murnane, Science **348**, 530 (2015).
[5] M. M. Seibert, T. Ekeberg, F. R. N. C. Maia, M. Svenda, J. Andreasson, O. Jonsson, D. Odic, B. Iwan, A. Rocker, D. Westphal, M. Hantke, D. P. DePonte, A. Barty, J. Schulz, L. Gumprecht, N. Coppola, A. Aquila, M. N. Liang, T. A. White, A. Martin, C. Caleman, S. Stern, C. Abergel, V. Seltzer, J. M. Claverie, C. Bostedt, J. D. Bozek, S. Boutet, A. A. Miahnahri, M. Messerschmidt, J. Krzywinski, G. Williams, K. O. Hodgson, M. J. Bogan, C. Y. Hampton, R. G. Sierra, D. Starodub, I. Andersson, S. Bajt, M. Barthelmess, J. C. H. Spence, P. Fromme, U. Weierstall, R. Kirian, M. Hunter, R. B. Doak, S. Marchesini, S. P. Hau-Riege, M. Frank, R. L. Shoeman, L. Lomb, S. W. Epp, R. Hartmann, D. Rolles, A. Rudenko, C. Schmidt, L. Foucar, N. Kimmel, P. Holl, B. Rudek, B. Erk, A. Homke, C. Reich, D. Pietschner, G. Weidenspointner, L. Struder, G. Hauser, H. Gorke, J. Ullrich, I. Schlichting, S. Herrmann, G. Schaller, F. Schopper, H. Soltau, K. U. Kuhnel, R. Andritschke, C. D. Schroter, F. Krasniqi, M. Bott, S. Schorb, D. Rupp, M. Adolph, T. Gorkhover, H. Hirsemann, G. Potdevin, H. Graafsma, B. Nilsson, H. N. Chapman, and J. Hajdu, Nature **470**, 78 (2011).
[6] N. D. Loh, C. Y. Hampton, A. V. Martin, D. Starodub, R. G. Sierra, A. Barty, A. Aquila, J. Schulz, L. Lomb, J. Steinbrener, R. L. Shoeman, S. Kassemeyer, C. Bostedt, J. Bozek, S. W. Epp, B. Erk, R. Hartmann, D. Rolles, A. Rudenko, B. Rudek, L. Foucar, N. Kimmel, G. Weidenspointner, G. Hauser, P. Holl, E. Pedersoli, M. Liang, M. M. Hunter, L. Gumprecht, N. Coppola, C. Wunderer, H. Graafsma, F. R. N. C. Maia, T. Ekeberg, M. Hantke, H. Fleckenstein, H. Hirsemann, K. Nass, T. A. White, H. J. Tobias, G. R. Farquar, W. H. Benner, S. P. Hau-Riege, C. Reich, A. Hartmann, H. Soltau, S. Marchesini, S. Bajt, M. Barthelmess, P. Bucksbaum, K. O. Hodgson, L. Struder, J. Ullrich, M. Frank, I. Schlichting, H. N. Chapman, and M. J. Bogan, Nature **486**, 513 (2012).
[7] C. Kupitz, S. Basu, I. Grotjohann, R. Fromme, N. A. Zatsepin, K. N. Rendek, M. S. Hunter, R. L. Shoeman, T. A. White, D. J. Wang, D. James, J. H. Yang, D. E. Cobb, B. Reeder, R. G. Sierra, H. G. Liu, A. Barty, A. L. Aquila, D. Deponte, R. A. Kirian, S. Bari, J. J. Bergkamp, K. R. Beyerlein, M. J. Bogan, C. Caleman, T. C. Chao, C. E. Conrad, K. M. Davis, H. Fleckenstein, L. Galli, S. P. Hau-Riege, S. Kassemeyer, H. Laksmono, M. N. Liang, L. Lomb, S. Marchesini, A. V. Martin, M. Messerschmidt, D. Milathianaki, K. Nass, A. Ros, S. Roy-Chowdhury, K. Schmidt, M. Seibert, J. Steinbrener, F. Stellato, L. F. Yan, C. Yoon, T. A. Moore, A. L. Moore, Y. Pushkar, G. J. Williams, S. Boutet, R. B. Doak, U. Weierstall, M. Frank, H. N. Chapman, J. C. H. Spence, and P. Fromme, Nature **513**, 261 (2014).
[8] J. R. Fienup, Appl. Opt. **21**, 2758 (1982).
[9] S. Marchesini, Rev. Sci. Instrum. **78**, 011301 (2007).
[10] S. Marchesini, H. He, H. N. Chapman, S. P. Hau-Riege, A. Noy, M. R. Howells, U. Weierstall, and J. C. H. Spence, Phys. Rev. B **68**, 140101(R) (2003).
[11] M. F. Hantke, D. Hasse, F. R. N. C. Maia, T. Ekeberg, K. John, M. Svenda, N. D. Loh, A. V. Martin, N. Timneanu, D. S. D. Larsson, G. van der Schot, G. H. Carlsson, M. Ingelman, J. Andreasson, D. Westphal, M. N. Liang, F. Stellato, D. P. DePonte, R. Hartmann, N. Kimmel, R. A. Kirian, M. M. Seibert, K. Muhlig, S. Schorb, K. Ferguson, C. Bostedt, S. Carron, J. D. Bozek, D. Rolles, A. Rudenko, S. Epp, H. N. Chapman, A. Barty, J. Hajdu, and I. Andersson, Nat. Photonics **8**, 943 (2014).
[12] T. Kimura, Y. Joti, A. Shibuya, C. Y. Song, S. Kim, K. Tono, M. Yabashi, M. Tamakoshi, T. Moriya, T. Oshima, T. Ishikawa, Y. Bessho, and Y. Nishino, Nat. Commun. **5**, 3052 (2014).
[13] G. van der Schot, M. Svenda, F. R. N. C. Maia, M. Hantke, D. P. DePonte, M. M. Seibert, A. Aquila, J. Schulz, R. Kirian, M. Liang, F. Stellato, B. Iwan, J. Andreasson, N. Timneanu, D. Westphal, N. F. Almeida, D. Odic, D. Hasse, G. H. Carlsson, D. S. D. Larsson, A. Barty, A. V. Martin, S. Schorb, C. Bostedt, J. D. Bozek, D. Rolles, A. Rudenko, S. Epp, L. Foucar, B. Rudek, R. Hartmann, N. Kimmel, P. Holl, L. Englert, N. T. D. Loh, H. N. Chapman, I. Andersson, J. Hajdu, and T. Ekeberg, Nat. Commun. **6**, 5704 (2015).
[14] H. J. Park, N. D. Loh, R. G. Sierra, C. Y. Hampton, D. Starodub, A. V. Martin, A. Barty, A. Aquila, J. Schulz, J. Steinbrener, R. L. Shoeman, L. Lomb, S. Kassemeyer, C. Bostedt, J. Bozek, S. W. Epp, B. Erk, R. Hartmann, D. Rolles, A. Rudenko, B. Rudek, L. Foucar, N. Kimmel, G. Weidenspointner, G. Hauser, P. Holl, E. Pedersoli, M. Liang, M. S. Hunter, L. Gumprecht, N. Coppola, C. Wunderer, H. Graafsma, F. R. N. C. Maia, T. Ekeberg, M. Hantke, H. Fleckenstein, H. Hirsemann, K. Nass, H. J. Tobias, G. R. Farquar, W. H. Benner, S. Hau-Riege, C. Reich, A. Hartmann, H. Soltau, S. Marchesini, S. Bajt, M. Barthelmess, L. Strueder, J. Ullrich, P. Bucksbaum, M. Frank, I. Schlichting, H. N. Chapman, M. J. Bogan, and V. Elser, Opt. Express **21**, 28729 (2013).
[15] G. P. Bewley, D. P. Lathrop, and K. R. Sreenivasan, Nature **441**, 588 (2006).
[16] L. F. Gomez, E. Loginov, and A. F. Vilesov, Phys. Rev. Lett. **108**, 155302 (2012).

[17]P. Thaler, A. Volk, F. Lackner, J. Steurer, D. Knez, W. Grogger, F. Hofer, and W. E. Ernst, Phys. Rev. B **90**, 155442 (2014).

[18]D. Spence, E. Latimer, C. Feng, A. Boatwright, A. M. Ellis, and S. F. Yang, Phys. Chem. Chem. Phys. **16**, 6903 (2014).

[19]E. Latimer, D. Spence, C. Feng, A. Boatwright, A. M. Ellis, and S. F. Yang, Nano Lett. **14**, 2902 (2014).

[20]L. F. Gomez, K. R. Ferguson, J. P. Cryan, C. Bacellar, R. M. P. Tanyag, C. Jones, S. Schorb, D. Anielski, A. Belkacem, C. Bernando, R. Boll, J. Bozek, S. Carron, G. Chen, T. Delmas, L. Englert, S. W. Epp, B. Erk, L. Foucar, R. Hartmann, A. Hexemer, M. Huth, J. Kwok, S. R. Leone, J. H. S. Ma, F. R. N. C. Maia, E. Malmerberg, S. Marchesini, D. M. Neumark, B. Poon, J. Prell, D. Rolles, B. Rudek, A. Rudenko, M. Seifrid, K. R. Siefermann, F. P. Sturm, M. Swiggers, J. Ullrich, F. Weise, P. Zwart, C. Bostedt, O. Gessner, and A. F. Vilesov, Science **345**, 906 (2014).

[21]J. P. Toennies and A. F. Vilesov, Angew. Chem., Int. Ed. **43**, 2622 (2004).

[22]L. F. Gomez, E. Loginov, R. Sliter, and A. F. Vilesov, J. Chem. Phys. **135**, 154201 (2011).

[23]L. Strüder, S. Epp, D. Rolles, R. Hartmann, P. Holl, G. Lutz, H. Soltau, R. Eckart, C. Reich, K. Heinzinger, C. Thamm, A. Rudenko, F. Krasniqi, K. U. Kuhnel, C. Bauer, C. D. Schroter, R. Moshammer, S. Techert, D. Miessner, M. Porro, O. Halker, N. Meidinger, N. Kimmel, R. Andritschke, F. Schopper, G. Weidenspointner, A. Ziegler, D. Pietschner, S. Herrmann, U. Pietsch, A. Walenta, W. Leitenberger, C. Bostedt, T. Moller, D. Rupp, M. Adolph, H. Graafsma, H. Hirsemann, K. Gartner, R. Richter, L. Foucar, R. L. Shoeman, I. Schlichting, and J. Ullrich, Nucl. Instrum. Methods A **614**, 483 (2010).

[24]T. Gorkhover, M. Adolph, D. Rupp, S. Schorb, S. W. Epp, B. Erk, L. Foucar, R. Hartmann, N. Kimmel, K. U. Kuhnel, D. Rolles, B. Rudek, A. Rudenko, R. Andritschke, A. Aquila, J. D. Bozek, N. Coppola, T. Erke, F. Filsinger, H. Gorke, H. Graafsma, L. Gumprecht, G. Hauser, S. Herrmann, H. Hirsemann, A. Homke, P. Holl, C. Kaiser, F. Krasniqi, J. H. Meyer, M. Matysek, M. Messerschmidt, D. Miessner, B. Nilsson, D. Pietschner, G. Potdevin, C. Reich, G. Schaller, C. Schmidt, F. Schopper, C. D. Schroter, J. Schulz, H. Soltau, G. Weidenspointner, I. Schlichting, L. Strueder, J. Ullrich, T. Moller, and C. Bostedt, Phys. Rev. Lett. **108**, 245005 (2012).

[25]C. Bostedt, J. D. Bozek, P. H. Bucksbaum, R. N. Coffee, J. B. Hastings, Z. Huang, R. W. Lee, S. Schorb, J. N. Corlett, P. Denes, P. Emma, R. W. Falcone, R. W. Schoenlein, G. Doumy, E. P. Kanter, B. Kraessig, S. Southworth, L. Young, L. Fang, M. Hoener, N. Berrah, C. Roedig, and L. F. DiMauro, J. Phys. B **46**, 164003 (2013).

[26]See supplementary material at http://dx.doi.org/10.1063/1.4933297 for additional information about the DCDI algorithm and additional discussions.

[27]R. J. Donnelly, *Quantized Vortices in Helium II* (Cambridge University Press, Cambridge, 1991).

[28]E. J. Yarmchuk, M. J. V. Gordon, and R. E. Packard, Phys. Rev. Lett. **43**, 214 (1979).

[29]G. H. Bauer, R. J. Donnelly, and W. F. Vinen, J. Low Temp. Phys. **98**, 47 (1995).

[30]K. K. Lehmann and R. Schmied, Phys. Rev. B **68**, 224520 (2003).

[31]D. R. Tilley and J. Tilley, *Superfluidity and Superconductivity* (Institute of Physics Publishing, Bristol, 1990).

[32]G. W. Stroke, Appl. Phys. Lett. **6**, 201 (1965).

[33]S. Eisebitt, J. Luning, W. F. Schlotter, M. Lorgen, O. Hellwig, W. Eberhardt, and J. Stohr, Nature **432**, 885 (2004).

[34]S. Flewett, C. M. Gunther, C. V. Schmising, B. Pfau, J. Mohanty, F. Buttner, M. Riemeier, M. Hantschmann, M. Klaui, and S. Eisebitt, Opt. Express **20**, 29210 (2012).

[35]A. V. Martin, A. J. D'Alfonso, F. Wang, R. Bean, F. Capotondi, R. A. Kirian, E. Pedersoli, L. Raimondi, F. Stellato, C. H. Yoon, and H. N. Chapman, Nat. Commun. **5**, 5661 (2014).

[36]S. G. Podorov, K. M. Pavlov, and D. M. Paganin, Opt. Express **15**, 9954 (2007).

[37]M. Guizar-Sicairos and J. R. Fienup, Opt. Express **15**, 17592 (2007).

[38]B. L. Henke, E. M. Gullikson, and J. C. Davis, At. Data Nucl. Data Tables **54**, 181 (1993).

[39]M. Kerker, *The Scattering of Light and Other Electromagnetic Radiation* (Academic Press, New York, 1969).

[40]D. Attwood, *Soft X-Ray and Extreme Ultraviolet Radiation: Principles and Applications* (Cambridge University Press, Cambridge, 2000).

[41]F. Bierau, P. Kupser, G. Meijer, and G. von Helden, Phys. Rev. Lett. **105**, 133402 (2010).